Tellus (1999), 51A, 951–963
Printed in UK. All rights reserved

TELLUS
ISSN 0280–6495

Mountain-wave-induced record low stratospheric temperatures above northern Scandinavia

By ANDREAS DÖRNBRACK[1]*, MARTIN LEUTBECHER[1], RIGEL KIVI[2] and ESKO KYRÖ[2], [1]*DLR Oberpfaffenhofen, Institut für Physik der Atmosphäre, D-82230 Wessling, Germany;* [2]*Finnish Meteorological Institute, Ilmala, FIN-99600 Sodankylä, Finland*

(Manuscript received 11 September 1998; in final form 30 March 1999)

ABSTRACT

On 22 January 1997 1200 UT, the routine radiosonde from Sodankylä, Finland, measured a record low temperature of −94.5°C at 26 km. Mesoscale numerical simulations indicate strong mountain wave activity on this day. Two stratospheric temperature minima are simulated: one directly above the Scandinavian mountain ridge and another minimum in its lee about 500 km to the east. Both minima are not resolved in the global analyses. The radiosonde profile as well as the mesoscale model indicate that the eastern mesoscale temperature anomaly is caused by orographic inertia-gravity waves, i.e., hydrostatic mountain waves influenced by Coriolis force. Stratospheric ice clouds were observed visually and by ground-based lidar at Kiruna, Sweden and Sodankylä, Finland on this day. The formation of these ice clouds required the cooling in the mountain waves as the temperature according to global analyses was about 3 K above the frost point. The occurrence of additional polar stratospheric ice clouds due to mountain-wave cooling increases the efficiency of chlorine activation and has implications for the resulting Arctic ozone depletion. The extraordinary event under consideration occurred during a cold air outbreak with a cold front passing over the Scandinavian orography. This front was associated with strong winds in the lower troposphere. At the same time, northern Scandinavia was located below the inner edge of the polar vortex, where low synoptic-scale stratospheric temperatures and a strong polar night jet are found.

1. Motivation

Stratospheric clouds above Scandinavia have been observed since the 1870s (Stanford and Davies, 1974). A first step to explain the nature of these so-called mother-of-pearl clouds was the exact determination of their height range of 20, … , 30 km by Störmer (1929, 1931) in the 1920s. He also gave an estimate of the size of cloud constituents during an exceptional night-time observation of a rather homogeneous, translucent stratospheric cloud illuminated by the moon (Störmer, 1934). Based on measurements of the inner and outer halo diameter, Störmer estimated a maximum particle size of 25 μm, much less than the known particle size in tropospheric clouds at that time. Today, we know that ice particles in mother-of-pearl clouds are typically one order of magnitude smaller (1, … , 4 μm) (Deshler et al., 1994; Carslaw et al., 1998b).

Recently, scientific interest has focussed again on polar stratospheric clouds (PSCs)* because

* Corresponding author.
e-mail: andreas.doernbrack@dlr.de

* PSCs are classified in two main groups: PSCs of type II consist of water ice particles, form at temperatures about 4 K below the ice frost point T_{frost} (Carslaw et al., 1998a) and are identical to the mother-of-pearl clouds; PSCs of type I exist at higher temperatures and consist of nitric acid trihydrate (NAT).

chemical reactions on PSC particles play a major part in the depletion of the ozone layer. These reactions are very efficient at low temperatures due to the increase in particle surface area and in heterogeneous reaction rates (Peter, 1997).

Synoptically, minimum stratospheric temperatures are expected to be located close to the centre of the polar vortex due to radiative cooling during the polar night. The Arctic stratosphere, however, is frequently disturbed by transient planetary waves and the polar vortex is deformed and asymmetric. Thus, the stratospheric air is often too warm for the formation of PSCs on the synoptic scale (Pawson et al., 1995), and global models underestimate the ozone depletion in the Arctic (Carslaw et al., 1998a).

Therefore, mesoscale processes leading to large vertical displacements of stratospheric air masses are important for the formation of ice PSCs as the air cools adiabatically due to expansion in ascending regions. Internal gravity waves which are induced by airflow over mountains can propagate up to stratospheric levels. These mountain waves are considered as one of the main sources of large mesoscale temperature anomalies above land surfaces of the northern hemisphere (Nastrom and Fritts, 1992).

The cooling in mountain wave events rarely exceeds the order of 10 K (Leutbecher and Volkert, 1996, Carslaw et al., 1998a). Therefore, the formation of ice PSCs requires additionally low background temperatures. On the synoptic scale, planetary waves play a major rôle in controlling the stratospheric temperatures (Teitelbaum and Sadourny, 1998).

Here, we focus on the investigation of a particular case, the spectacular PSC event on 22 January 1997. The structure of mother-of-pearl clouds above the Scandinavian mountains documented on a photograph taken from Kiruna, Sweden, at 1300 UT (Fig. 1) already indicates the processes associated with their formation: the iridescent clouds resemble tropospheric *lenticularis* clouds forming at the crests of trapped leewaves. In spite of the strong winds, the mother-of-pearl clouds did not show any significant downwind advection, a typical sign of mountain-wave induced clouds.

The aim of this study is to analyse the meteorological conditions that lead to very low stratospheric temperatures over Scandinavia. In Section 2, technical details of the observations and the mesoscale model set-up are given. The radiosonde soundings are presented in Section 3. The mesoscale model results are discussed and compared with observations in Section 4. Finally, the large-scale synoptic situation is examined and conclusions are drawn in Section 5.

2. Methodology

In this study, high-vertical-resolution radiosonde soundings, lidar data, mesoscale numerical modelling and global analyses by the European Centre for Medium-Range Weather Forecasts (ECMWF) are combined to explain observations of PSCs above Kiruna and Sodankylä on 22 January 1997.

The 12 hourly routine soundings at Sodankylä are recorded by a Väisälä RS 80 sonde with a frequency of 0.5 Hz, i.e., a vertical resolution of approximately 10 m (assuming a mean constant balloon ascent rate of 5 m/s). The accuracy of horizontal wind speed calculations by the Omega system is about 2.5 m/s (Nash, 1994). The accuracy (reproducibility) of the RS 80 temperature sensor is 0.3 K between 50 and 15 hPa. Hence, accuracy of the altitude calculations is ± 20 m at this altitude range, allowing resolution of thin vertical layers with these fine-vertical-resolution radiosonde profiles.

The weather prediction model MM5 (Dudhia, 1993; Grell et al., 1994) is used to simulate the three-dimensional mesoscale flow over the Scandinavian mountains during the period of PSC observations. The model integrates the fully compressible set of equations in a rotating frame of reference. In the non-hydrostatic version used here, velocity, pressure perturbation and temperature are the prognostic variables.

The model domain is centred around central Scandinavia (65°N, 15°E) with an extension of 2196 km × 2196 km. A local grid refinement (nested domain of 984 km × 984 km) covering the northern part of the Scandinavian mountain ridge around its peak Kebnekaise (67°54′ N, 18°30′ E) is used to resolve most of the spectrum of vertically propagating gravity waves generated by the orography. The horizontal mesh size of the outer domain is $\Delta x = 36$ km, the grid length of the nested domain amounts to 12 km. Thus, a distance

Fig. 1. Polar stratospheric clouds (mother-of-pearl clouds) on 22 January 1997. Photograph taken at Kiruna, Sweden, looking south-west at 1300 UT. The airflow is from right (west) to left (east). Courtesy of Anne Réchou, Swedish Institute of Space Physics, Kiruna.

of about 1000 km lies between the lateral boundaries and the mountain region. This diminishes the interaction between the orographically induced airflow and the domain boundaries. Terrain heights on the finest grid were obtained by interpolation from a 30″ orographic data set provided by the Geophysical Data Center (Boulder). According to estimates of Leutbecher (1998), the shortest horizontal wavelength resolved by the numerical model is about $10\Delta x = 120$ km for gravity waves that have propagated into the stratosphere.

The vertical resolution Δz amounts to approximately 570 m. In total, 52 levels are used up to the model top at 10 hPa (≈ 28 km). There, a radiative boundary condition avoids the reflection of vertically propagating gravity waves. Radiative and moist processes are switched off as the prime concern lies in the dynamics of mountain waves at upper levels.

The initial conditions and boundary values of the model integration were prescribed by 12 hourly analyses of the ECMWF with a horizontal resolution of 2.5° in latitude and longitude and 15 levels between the surface and the 10 hPa pressure level (Dörnbrack et al., 1998).

3. Observations

In the period from 20 to 26 January 1997, a sequence of deep tropospheric lows north of Scandinavia (minimum core pressure 960 hPa on 21 January near Spitsbergen) led to long-lasting westerly, north-westerly low-level winds with average speeds greater than 10 m/s (in gusts more than 25 m/s)*

At Andøya, Norway, on the windward side of the mountains, the gale and heavy snow fall starting during the night of 21 January prevented PSC observations during the subsequent days. Downwind of the mountains, the descending dry air enabled, at least from time to time, ground-based visual (such as Fig. 1) as well as the remote sensing observations on 22 January 1997.

The University of Bonn backscatter lidar at Esrange near Kiruna detected ice clouds with backscatter ratios** $S > 110$ at an altitude of $z = 25$ km for a couple of minutes at about 1100 UT. In the afternoon (1425 till 2128 UT), the backscatter ratio S remained below 15. Fricke et al. (1997) reported about PSCs in the altitude range 23 to 27 km.

At Sodankylä, about 350 km east of Kiruna, the evolution of PSCs could be recorded by a ground based lidar for about 12 h. The first PSC was observed between 0130 and 0400 UT on 22 January with a maximum backscatter ratio of about 50 (in the 532 nm channel) at an altitude of about 23 km. The high values of backscatter ratio as well as the large depolarization factor of about 13% point to ice particles (PSC of type II). At 2045 UT, a PSC type II was sampled by a balloon-borne backscatter sonde at an elevation

* Archived weather information from the University of Tromsø, Norway, is available via internet: http://www.cs.uit.no/cgi-bin/weather.

** $S = (\beta_{\text{aeroso}} + \beta_{\text{air}})/\beta_{\text{air}}$, where β is the backscatter coefficient at 532 nm in the parallel channel.

between 25 and 26.5 km. Further lidar measurements starting at 2100 UT detected PSCs in a height range of 23 to 27 km (Kivi et al., 1998).

The regular radiosonde of Sodankylä launched at 1200 UT on 22 January 1997 observed a minimum temperature of 178.6 K between 25 and 26 km, i.e. ≈ 17 hPa (Fig. 2). This is the lowest stratospheric temperature recorded during the winter 1996/97 and one of the lowest temperatures ever measured in-situ in the stratosphere. Moreover, the record low temperature of 22 January 1997 was the coldest stratospheric temperature in the 35 years database of regular radiosoundings at Sodankylä.

Climatological time series of synoptic-scale analyses by Pawson et al. (1995) and NCEP (Coy et al., 1997*) provide further evidence that the measured temperature of 178.6 K is extremely low for the Arctic stratosphere. The Arctic minimum stratospheric temperature of 29 (NCEP) or 10 (Pawson), of previous years of daily analyses, is 181 K.

The other striking feature of this radiosonde ascent is the vertical succession of layers with alternating values of high and low static stability above the tropopause. There are three 2, ..., 3 km thick inversion layers ($\Delta T/\Delta z \approx +1$ K/km) around 13, 21 and 27 km, where the buoyancy frequency $N = \sqrt{g/\theta \, \mathrm{d}\theta/\mathrm{d}z}$ (where θ is the potential temperature) is increased drastically to values much larger than the typical stratospheric values of $N = 0.02\ \mathrm{s}^{-1}$. The apparent vertical wavelength of these variations (see $N(z)$ in Fig. 2) amounts to about 7 km. Above the inversion layers, the lapse rate is 4 to 5 K/km and in the mean, N is much smaller than $0.02\ \mathrm{s}^{-1}$. The 1900 UT backscatter sonde recorded a minimum temperature of about 181 K at 26 km. However, the vertically extended layers of high static stability had disappeared.

Vertical variations also occur in the wind speed and direction of the radiosonde ascent that measured the record low temperature (Fig. 3). Above 13 km, wind speed and direction oscillate periodically with a vertical wavelength similar to that of the temperature profile. The peak-to-peak amplitudes are ≈ 35 m/s and $\approx 30^\circ$, respectively. The wind attained values of about 20 m/s at an altitude of 1 km and a strong tropospheric jet of 75 m/s was observed between 8 and 11 km.

Upstream temperature and wind observations for levels above 70 hPa are only available from Jan Mayen (70.6°N, 8.4°W) at 1200 UT. There, wavelike oscillations appear neither in the temperature nor in the velocity profile. The most remarkable feature is a cold layer of 188 K at 28 hPa (≈ 23 km) between warmer air below and above (191 K at 30 hPa and 192 K at 23 hPa).

In hodographs of the 22 January 0000 UT and 1200 UT ascents of Sodankylä, an anticyclonic turning of the wind vector with increasing height (veering) is apparent above the tropopause (Fig. 4). This phase relation between the perturbations of the u and v components is an indication of inertia-gravity waves that propagate energy upward (Gill, 1982). In a frame of reference moving with the flow, the phase propagation is downward. The hodograph on 23 January 0000 UT shows only a little sign of mountain wave influence. This is due to weaker excitation of mountain waves in the preceding 12 h, because the high low-level winds ceased rapidly.

The Scandinavian ridge has a sufficient width to excite inertia-gravity waves that propagate considerably downstream on their way into the stratosphere, and thus cause the oscillations of temperature and wind in the 1200 UT ascent of Sodankylä. Estimating the vertical wavelength for homogeneous upstream conditions on 22 January 0000 UT given by a wind speed $\bar{V}_\mathrm{H} = 30\ \mathrm{ms}^{-1}$ and a buoyancy frequency $\bar{N} = 0.02\ \mathrm{s}^{-1}$ yields a value of $\lambda_z^* = 2\pi \bar{V}_\mathrm{H}/\bar{N} \approx 9.5$ km, where a hydrostatic, two-dimensional flow without background rotation is assumed for the estimate. Coriolis effects reduce the vertical wavelength by a factor of $[1 - ((1/2\pi) f \lambda_x/\bar{V})^2]^{1/2}$. For horizontal wavelengths of $\lambda_x = 500$ km and 1000 km, the reductions amounts to 0.94 and 0.72, respectively. The vertical wavelength apparent in the radiosonde ascent is somewhat smaller. The buoyancy profile and the hodograph reveal a wavelength of about 7 km (Figs. 2, 4). Assuming that the phaselines of encountered waves tilt upstream corresponding to an upward energy propagation, the apparent wavelength in the slant radiosonde ascent is shorter than the actual vertical wavelength (Shutts et al., 1988). The inclination of the path of the sonde to the horizontal is about 5:30. For a

* A complete set of meteorological information of the stratospheric state is available via the internet site of the National Center of Environmental Prediction (NCEP): http://www.ncep.noaa.gov.

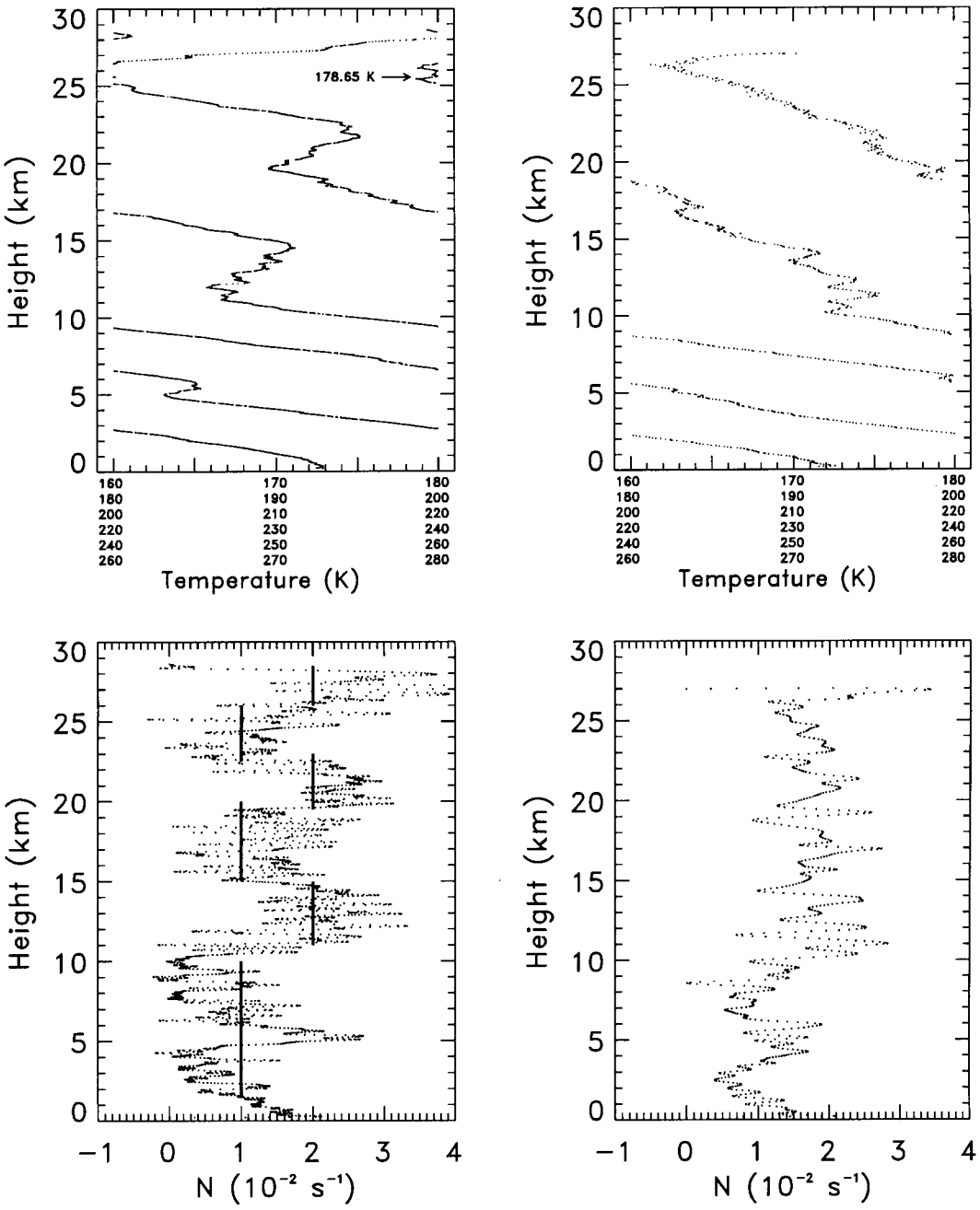

Fig. 2. High-vertical-resolution soundings at Sodankylä, Finland on 22 January 1997: Temperature T (K; scale folded every 20 K; at the ground 272 K; top row) and buoyancy frequency N ($10^{-2}\,s^{-1}$; bottom row). The regular radiosonde was launched at 1137 UT (temporal resolution of 2 s, 2817 values; left column) and the backscatter sonde at 1906 UT (temporal resolution 7 s, 775 values; right column).

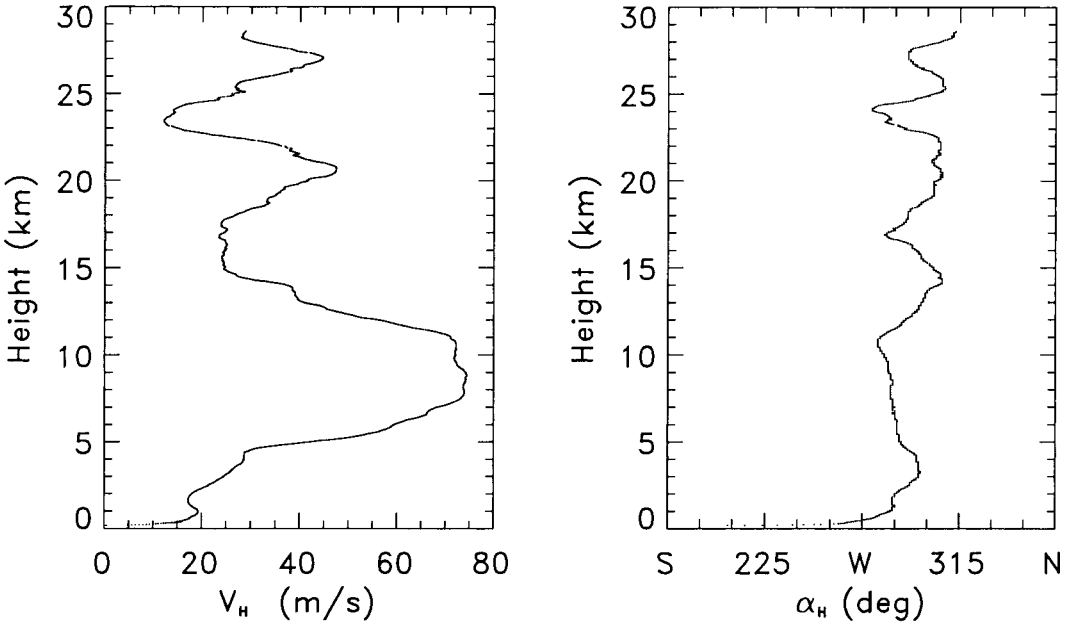

Fig. 3. High-vertical-resolution sounding at Sodankylä, Finland on 22 January 1997 1137 UT: wind speed V_H (m/s; left) and wind direction α_H (deg/right).

horizontal wavelength of about 500 km, the corrected vertical wavelength is around 7.5 km = $0.79\lambda^*$. Therefore, the oscillations in the 1200 UT ascent of Sodankylä are consistent with inertia-gravity waves that have horizontal wavelengths of the order of magnitude of 500 km.

To improve the understanding of the observed features, mesoscale numerical simulations are presented next.

4. Model results

In the numerical simulation, the flow past the Scandinavian ridge excites gravity waves that propagate vertically. This results in stratospheric perturbations aloft and downstream of the Scandinavian ridge. The wave structure of mesoscale temperature anomalies resembles the pattern of other cases, but the duration and amplitude of the mountain wave events are different (Leutbecher and Volkert, 1996; Wirth et al., 1999).

Fig. 5 juxtaposes the simulated temporal evolution of profiles of temperature, buoyancy frequency and wind speed at the upstream location Andøya and the downstream location Sodankylä. Above Andøya, a layer of $T < 190$ K is found in an altitude range between 21 and 24 km with minimum temperatures below 188 K at $z = 23$ km as observed above Jan Mayen. The stratospheric temperature increases weakly during the afternoon of 22 January. The slowly descending tropopause appears as a sharp increase of the buoyancy frequency N at $z \approx 10$ km. In the night of 21 January, the tropospheric jet is most pronounced with speeds greater than 80 m/s at $z =$ 9 km. The wind speed decreases throughout the troposphere including the jet in the course of 22 January 1997.

In contrast, the maximum wind speed above Sodankylä occurs about 9 h later. In the stratosphere, the wind speed oscillates at a vertical wavelength of about 9 km as the radiosonde profile on 22 January 1997 which is shown in Fig. 3. The simulated peak-to-peak amplitude of the wind speed amounts to 40 m/s. Minimum stratospheric temperatures are vertically confined between layers of enhanced static stability N, and their locations coincide with reduced horizontal wind speeds. According to the model, the most significant mountain-wave induced cooling above Sodankylä takes place between 0000 and 1200 UT

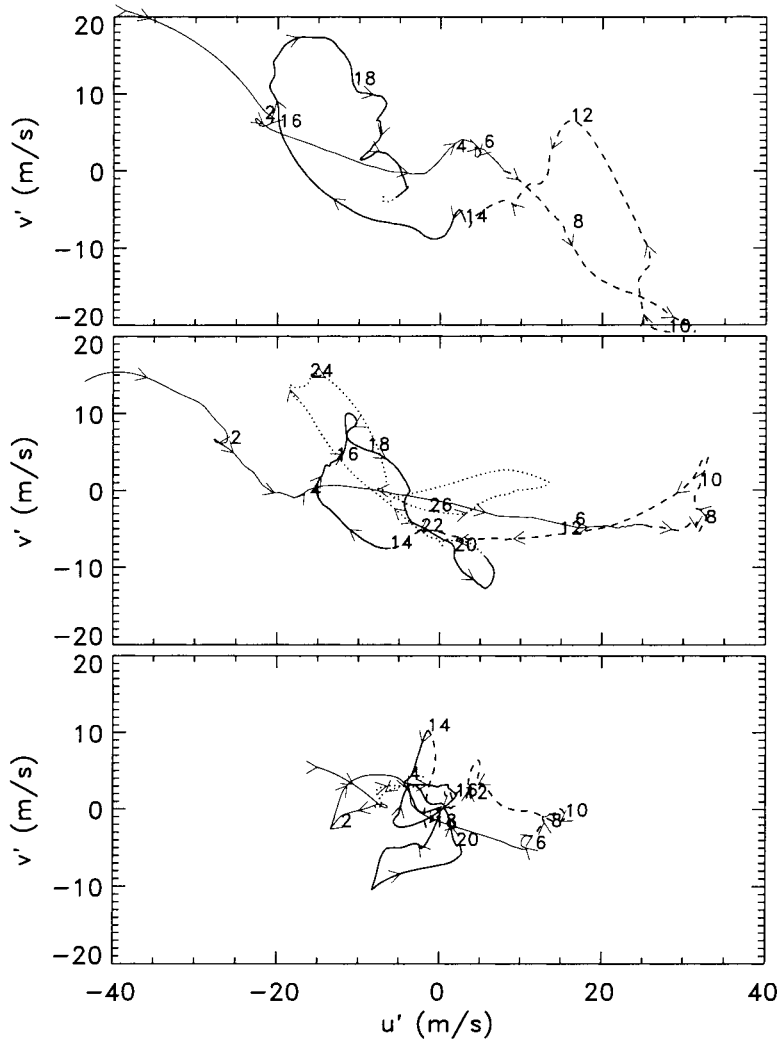

Fig. 4. Hodographs derived from velocity records of three high-vertical-resolution radiosonde soundings at Sodankylä on 22 January 0000 UT (top), 1200 UT (middle), and on 23 January 1997 0000 UT (bottom). The altitude is marked in 2 km intervals. The velocity perturbations of the meridional and zonal components u' and v' (m/s) are calculated as deviations from a linear regression.

when the temperatures around $z = 22$ km fall below T_{frost} (5 ppmv water vapor were assumed using the relations of Hanson and Mauersberger (1988)). Supercooled regions where the local temperature falls about 4 K below T_{frost} are necessary for the condensation of solid particles in ice PSCs (Carslaw et al., 1998a, b). The simulated temperature falls approximately 2.5 K below T_{frost}. This discrepancy between measurement and simulation of about 2 K could be caused inter alia by the known positive temperature bias of 2 to 3 K of the ECMWF analyses at stratospheric levels (Knudsen et al., 1996).

The simulated height of minimum temperature agrees well with the altitude of maximum backscatter (i.e., supercooled water ice particles) recorded by the ground based lidar in the morning, but not with the radiosonde temperature profile at 1200 UT as shown in Fig. 3. The three-dimensional stratospheric temperature distribution at

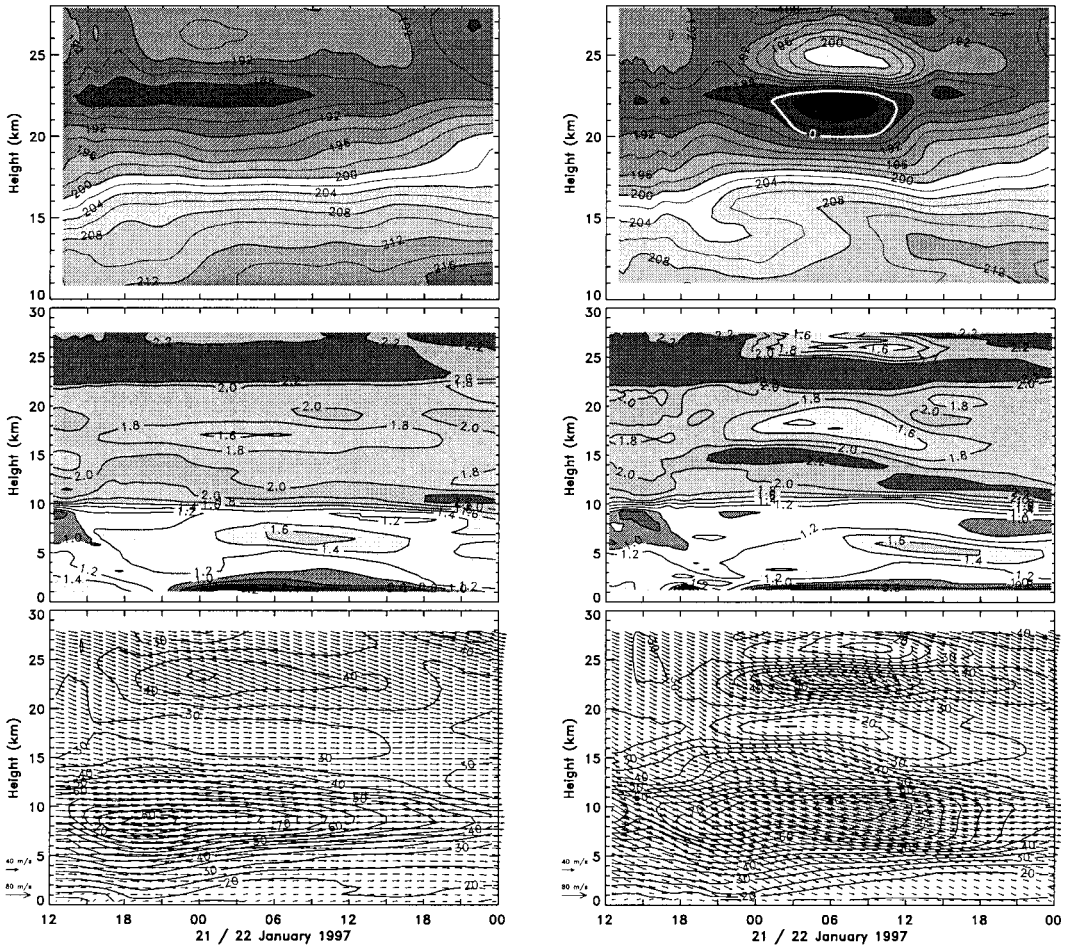

Fig. 5. Height-time sections of temperature (K; top), buoyancy frequency ($10^{-2}\,s^{-1}$; middle) and wind speed (m/s; bottom) at Andøya (left column) and Sodankylä (right column). Arrows pointing right (down) correspond to westerly (northerly) flow. Data are taken every 30 s from mesoscale model results. The white contour line in the temperature panel encloses the region where the temperature drops below T_{frost}.

0000 UT and 1200 UT is illustrated in Fig. 6 by a horizontal (at $z = 26$ km) and a vertical west-east section along the prolonged base line Kiruna — Sodankylä. At 0000 UT, a mesoscale temperature anomaly appears directly above the highest peak of the model orography as an isolated, elongated and coherent cold spot of about 100 km east-west extension with minimum temperatures of less than 178 K. The north-south extension of the cold anomalies amounts to approximately 400 km (Fig. 6a).

The maximum temperature decrease of 13 K on the 580 K isentropic surface (related to the upstream temperatures at the same level) results from the adiabatic expansion of ascending air. In the coldest region, the isentropic surface is vertically displaced by 1400 m (Fig. 6b). On the eastern as well as on the western side of the mesoscale temperature anomaly, warm regions with similar west-east extension are generated by descending air. At 1200 UT, a second cold region has been developed about 500 km downstream.

It is this cold spot, located about 200 km downwind of Sodankylä, where the radiosonde observed the record low temperature. Fig. 7 shows a comparison between the measured profile with two

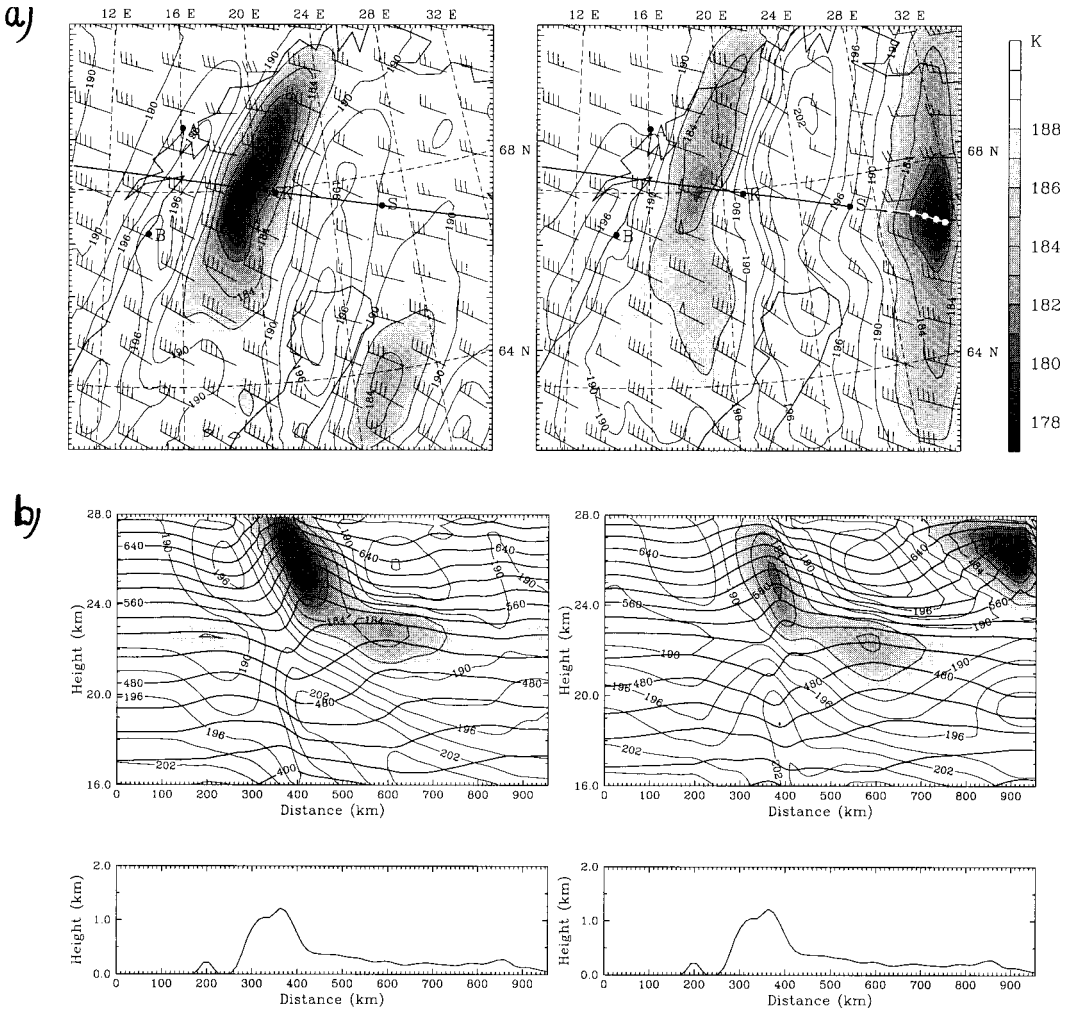

Fig. 6. (a) Mesoscale model temperature (K), horizontal wind vectors (barbs in ms^{-1}) at $z = 26$ km on 22 January 1997 0000 UT (left) and 1200 UT (right). The black line indicates the vertical cross sections (Fig. 6b). The balloon trajectory of the 1200 UT sounding is drawn in white and labeled by bullets every 5 km in altitude. Locations: Bodø (B), Kiruna (K), Andøya (A), Sodankylä (S). (b) Vertical section of the mesoscale model temperature (K; thin solid contours and grey shading) and the potential temperature (K; thick solid lines) on 22 January 1997 0000 UT (left) and 1200 UT (right). Bottom: Terrain height along the section base line.

profiles derived from the mesoscale simulations. The vertical temperature profile above Sodankylä shows a temperature minimum at $z = 23$ km and a maximum aloft as already indicated in Fig. 5. The profile following the actual balloon trajectory (the white line in Fig. 6a) matches the temperature minimum at $z = 26$ km. Thus, the agreement of the simulated and the observed stratospheric temperature minima improves significantly if the model data are taken along the balloon trajectory instead of a vertical profile. Furthermore, the location of the simulated eastern mesoscale temperature anomaly 200 km downwind of Sodankylä at an altitude of 26 km agrees with the balloon-borne backscatter observation of PSCs in that region. In the morning session of the ground-based lidar, PSCs were detected about 3 km lower.

The radiosonde of Bodø on 22 January 0000 UT

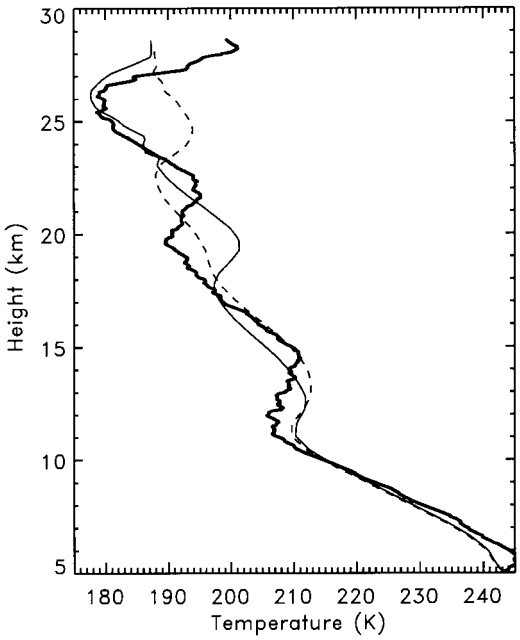

Fig. 7. Observed and simulated temperature profiles above Sodankylä at 1200 UT during the mountain wave event of 22 January 1997: fine-resolution radiosonde measurement (thick line); vertical profile of the mesoscale model straight above Sodankylä (dashed line); and model temperature along the actual balloon trajectory (thin line).

burst below an altitude of 20 km and did not reach the simulated temperature minimum above the ridge. The radiosonde of Bodø at 1200 UT that day got to the 20 hPa level and measured a minimum temperature of 182.5 K. This value is close to the simulated temperature minimum at 1200 UT above the ridge (Fig. 6a).

The veering of the wind vector in the observations as well as the retarded appearance of the downstream temperature minimum in the mesoscale simulations indicates that this feature is caused by slant propagation of internal gravity waves under the action of the Coriolis force (Queney, 1948; Gill, 1982). For mean conditions $\bar{N} = 0.02\ \mathrm{s}^{-1}$ and $\bar{V}_\mathrm{H} = 30\ \mathrm{ms}^{-1}$, the propagation time t_p of a gravity wave from the surface to an altitude of $z = 26$ km can be estimated by

$$t_\mathrm{p} = \frac{z}{c_{gz}} \approx 0.1\lambda_z\ \mathrm{sm}^{-1};$$

the vertical component of the group velocity c_{gz} for hydrostatic mountain waves in the non-rotating regime is given by

$$c_{gz} = \frac{\omega^2}{\bar{N}k_\mathrm{H}} = \frac{\bar{V}_\mathrm{H}^2 k_\mathrm{H}}{\bar{N}},$$

where k_H is the horizontal component of the wave vector (Gill, 1982, ch. 8.4). This means the propagation time t_p is proportional to the horizontal wavelength $\lambda_\mathrm{H} = 2\pi/k_\mathrm{H}$. For vertically-propagating hydrostatic waves of $\lambda_x \approx 50$ km, t_p is about 1.4 h. The horizontal wavelength of the mountain waves in Fig. 6 is about 400 km, i.e. $t_\mathrm{p} \approx 12$ h. Additionally, the vertical group velocity c_{gz} of long hydrostatic mountain waves in the rotating regime, is modified by a factor

$$\left(1 - \frac{f^2}{\bar{V}_\mathrm{H}^2 k_\mathrm{H}^2}\right)^{1.5},$$

which gives corrections for c_{gz} and t_p less than 12% for $\lambda_x < 400$ km, assuming $f = 1.3 \times 10^{-4}\ \mathrm{s}^{-1}$. Hence, the retarded appearance of the eastern temperature minimum can be explained by the long horizontal wavelength of the waves that caused the minimum.

5. Discussion and conclusions

The potential to form PSCs is frequently related to the location of synoptic-scale cold areas (Pawson et al., 1995, Coy et al., 1997). Fig. 8 shows the temperature distribution, the horizontal wind and the potential vorticity deduced from ECMWF analyses on the 550 K isentropic surface for 4 consecutive times starting at 21 January 1997 1200 UT with an interval of 12 h. The cold centre of the polar vortex is located over northern Scandinavia and the edge of the polar vortex (here, fixed as a potential vorticity belt of $70 \pm 5 \times 10^{-6}\ \mathrm{Km^2\,s^{-1}\,kg^{-1}}$) moves north during the period of 36 h. This leads to a state of the stratospheric flow, where the cold centre is horizontally displaced from the core of the polar vortex. At the inner edge of the polar vortex, a synoptic situation evolves where high horizontal winds exist within the cold areas. Simultaneously, strong low-level winds excite gravity waves which propagate without any significant absorption up to stratospheric levels. This leads to optimum conditions for extra mountain wave cooling.

Lidar measurements during the recent Arctic

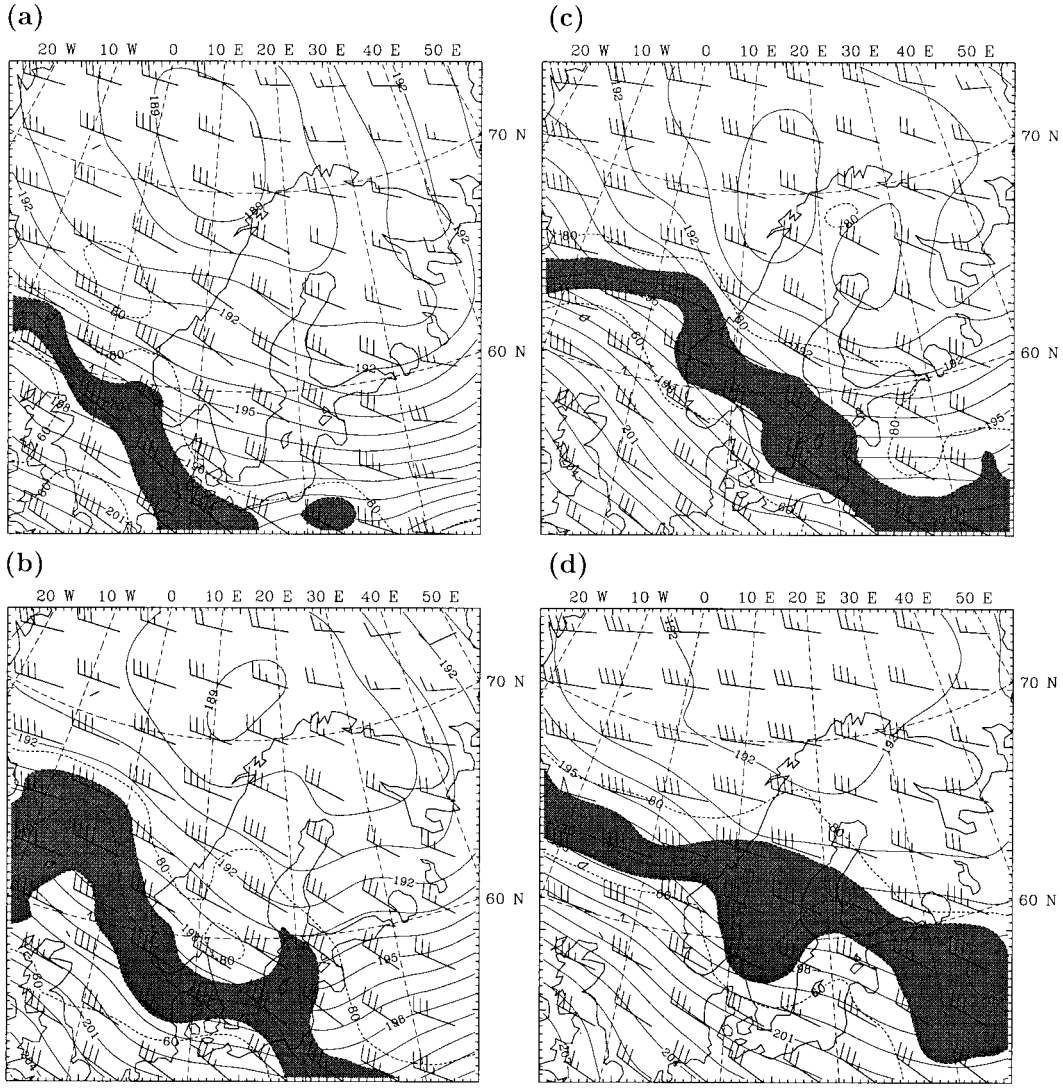

Fig. 8. Synoptic scale temperature (K; thin solid lines and grey shading as in Fig. 6), horizontal wind vectors (long/short barb: 10/5 ms^{-1}), and potential vorticity (10^{-6} $Km^2 s^{-1} kg^{-1}$; dashed) on the 550 K potential temperature surface at 21 January 1200 UT (a), 22 January 0000 UT (b), 1200 UT (c) and 23 January 0000 UT (d). The grey band indicates the boundary of the polar vortex. Data are taken from ECMWF analyses.

winters by Whiteway et al. (1997) give evidence that maximum stratospheric wave activity is strongly correlated with a westerly jet at the edge of the polar vortex. Whether this particular stratospheric state indirectly induces those tropospheric cold fronts that excite the mountain waves, remains an open question. Techniques as proposed by Hartley et al. (1998), who presented evidence of a feedback of the stratospheric flow field to the meteorological processes in the troposphere, may be applied to analyse such links.

In summary, the record low stratospheric temperatures observed on 22 January 1997 were produced under conditions where a cold stratosphere

on the synoptic scale coincided with strong mountain wave activity. On the synoptic scale, the minimum temperatures above Northern Scandinavia were around 190 K on that day according to ECMWF analyses (Fig. 8). This is still 9 K warmer than the lowest temperatures of the Arctic stratosphere found in the climatological series of synoptic scale analyses of the Pawson et al. (1995) and NCEP. The mesoscale cooling in the mountain wave amounts up to 13 K according to the numerical simulation. This results in regions colder than 180 K. In particular T_{frost} was attained and ice clouds were formed. Hence, the mountain waves were an essential ingredient for the formation of PSC type II on this day. This confirms the early hypothesis, that mother-of-pearl clouds in the Arctic are preferentially associated with strong airflow over mountains (Dietrichs, 1950).

The observed cold spot with the record low temperature is located about 500 km downstream of the mountains. The analysis of the high-vertical-resolution radiosonde sounding and mesoscale numerical simulations suggest that orographic inertia-gravity waves have caused the local cooling. The available stratospheric temperature information derived from observations (radiosonde as well as backscatter ratio) agrees well with the mesoscale simulation results.

Similar to this mountain wave event, many others are likely to occur at the edge of the polar vortex where synoptic-scale temperatures are often marginal for PSC formation. Although the chlorine activation on the surface of PSC particles happens in a couple of minutes, it lasts of the order of several days (Carslaw et al., 1998a). Thus mesoscale mountain wave events may provide a mechanism to effect the Arctic ozone depletion on the synoptic scale. The generation of at least two temperature minima by one mountain ridge further increases the efficiency of chlorine activation by mountain wave cooling.

The observation of the record low temperature is based on routine radiosonde soundings at Sodankylä. Both the high vertical resolution and the great altitude range were necessary for the analysis in this study. In order to obtain a better coverage of stratospheric in-situ temperature observations up- and downstream of the Scandinavian mountains during the Arctic winter and spring, balloons of the routine radiosondes should be prepared in a way that they regularly reach altitudes greater than 25 km. In special observation periods, the multiple sounding technique as proposed by Shutts et al. (1994) should be applied to observe horizontal gradients of the temperature field.

6. Acknowledgements

This study was supported by the German Research ministry in the framework of the German Ozone Research Programme. We thank Hans Volkert for bringing the historical papers by Carl Störmer to our attention. We furthermore thank him, Karl-Heinrich Fricke (Universität Bonn) and Jens Reichardt (GKSS Geesthacht) for commenting on earlier versions of the manuscript.

REFERENCES

Carslaw, K. S., Wirth, M., Tsias, A., Luo, B. P., Dörnbrack, A., Leutbecher, M., Volkert, H., Renger, W., Bacmeister, J. T., Reimer, E. and Peter, T. 1998a. Increased stratospheric ozone depletion due to mountain-induced atmospheric waves. *Nature* **391**, 675–678.

Carslaw, K. S., Wirth, M., Tsias, A., Luo, B. P., Dörnbrack, A., Leutbecher, M., Volkert, H., Renger, W., Bacmeister, J. T. and Peter, T. 1998b. Particle microphysics and chemistry in remotely observed mountain polar stratospheric clouds. *J. Geophys. Res.* **103**, 5785–5796.

Coy, L., Nash, E. R. and Newman, P. A. 1997. Meteorology of the polar vortex: Spring 1997. *Geophys. Res. Lett.* **24**, 2693–2696.

Deshler, T., Peter, T., Müller, R. and Crutzen, P. J. 1994. The lifetime of leewave-induced ice particles in the Arctic stratosphere (1). Balloon-borne observations. *Geophys. Res. Lett.* **21**, 2473–2478.

Dietrichs, H. 1950. Über die Entstehung der Perlmutterwolken. *Meteorol. Rundschau* **3**, 208–213.

Dörnbrack, A., Leutbecher, M., Volkert, H. and Wirth, M. 1998. Mesoscale forecasts of stratospheric mountain waves. *Meteorol. Appl.* **5**, 117–126.

Dudhia, J. 1993. A non-hydrostatic version of the Penn State–NCAR mesoscale model: validation tests and simulation of an Atlantic cyclone and cold front. *Mon. Weather Rev.* **121**, 1493–1513.

Fricke, K.-H., Müller, K. P., Baumgarten, G. and Siebert, J. 1997. Koordinierte Feldmessungen zum Einfluss von Leewellen auf Wolkenfelder in der polaren Stratosphäre. Results presented at the *7th Statussemminar des Ozonforschungsprogrammes des BMBF*, 10 and

11 July, 1997 in Bonn. Available from: Physikalisches Institut der Universität Bonn, Nußallee 12, D-53115 Bonn, Germany.

Gill, A. E. 1982. *Atmosphere–ocean dynamics*. Academic Press, 662 pp.

Grell, G. A., Dudhia J. and Stauffer, D. R. 1994. A description of the *5th-generation Penn State/NCAR mesoscale model (MM5)*. Techn. Note 398, National Center for Atmospheric Research, Boulder, USA, 121 pp.

Hanson, D. and Mauersberger, K. 1988. Laboratory studies of the nitric acid trihydrate: implications for the south polar stratosphere. *Geophys. Res. Lett*. **15**, 855–858.

Hartley, D. E., Villarin, J. T., Black, R. X. and Davies, C. A. 1998. A new perspective on the dynamical link between the stratosphere and troposphere. *Nature* **391**, 471–474.

Kivi, R., Kyrö, E., Wedekind, C., Rontu, L., Dörnbrack, A., Stein, B., Wille, H., Mitev, V., Matthey, R., Rosen, J., Kjome, N., Rizi, V., Redaelli, G., Lazzarotto, B., Calpini, B., Del Guasta, M., Morandi, M., Stefanutti, L., Agostini, P., Antonelli, A., Rummukainen, M., Turunen, T. and Karhu, J. 1998. SAONAS activities at Sodankylä in winter 1996/1997. *Proc. 4th European Workshop on Polar stratospheric ozone*, Schliersee, Bavaria, Germany. Report of the European Comission EUR 18032 EN, 135–138.

Knudsen, B. M., Rosen, J. M., Kjome, N. T. and Whitten, A. T. 1996. Comparison of analysed stratospheric temperatures and calculated trajectories with long-duration balloon data. *J. Geophys. Res*. **101**, 19137–19145.

Leutbecher, M. 1998. *Die Ausbreitung orographisch angeregter Schwerewellen in die Stratosphäre — Lineare Theorie, idealisierte und realitätsnahe numerische Simulation*. PhD thesis, Ludwig-Maximilians-Universität München. Rep. FB-98-17, available from Deutsches Zentrum für Luft- und Raumfahrt, D 51170 Köln, Germany.

Leutbecher, M. and Volkert, H. 1996. Stratospheric temperature anomalies and mountain waves: A three-dimensional simulation using a multi-scale weather prediction model. *Geophys. Res. Lett*. **23**, 3329–3332.

Nash, J. 1994. Upper wind observing systems used for meteorological operations. *Annales Geophysicae* **12**, 691–710.

Nastrom, G. D. and Fritts, D. C. 1992. Sources of mesoscale variability of gravity waves. (I). Topographic excitation. *J. Atmos. Sci*. **49**, 101–110.

Pawson, S., Naujokat, B. and Labitzke, K. 1995. On the polar stratospheric cloud formation potential of the northern stratosphere. *J. Geophys. Res*. **100**, 23215–23225.

Peter, T. 1997. Microphysics and heterogeneous chemistry of polar stratospheric clouds. *Annu. Rev. Phys. Chem*. **48**, 785–822.

Queney, P. 1948. The problem of airflow over mountains: A summary of theoretical studies. *Bull. Am. Meteorol. Soc*. **29**, 16–27.

Shutts, G. J., Kitchen, M. and Hoare, P. H. 1988. A large amplitude gravity wave in the lower stratosphere detected by radiosonde. *Q. J. R. Meteorol. Soc*. **114**, 579–594.

Shutts, G. J., Healey, P. and Mobbs, S. D. 1994. A multiple sounding technique for the study of gravity waves. *Q. J. R. Meteorol. Soc*. **120**, 59–77.

Stanford, J. L. and Davies, J. S. 1974. A century of stratospheric cloud reports: 1870–1972. *Bull. Am. Meteorol. Soc*. **55**, 213–219.

Störmer, C. 1929. Remarkable clouds at high altitudes. *Nature* **123**, 940–941.

Störmer, C. 1931. Höhe und Farbverteilung der Perlmutterwolken. *Geofysiske Publikasjoner* **IX**, 3–25.

Störmer, C. 1934. Höhenmessungen von Stratosphärenwolken. *Beitr. Phys. fr. Atmos*. **21**, 1–6.

Teitelbaum, H. and Sadourny, R. 1998. The role of planetary waves in the formation of polar stratospheric couds, *Tellus* **50A**, 302–312.

Whiteway, J. A., Duck, T. J., Donovan, D. P., Bird, J. C., Pal, S. R. and Carswell, A. I. 1997. Measurements of gravity wave activity within and around the Arctic stratospheric vortex. *Geophys. Res. Lett*. **24**, 1387–1390.

Wirth, M., Weiß, V., Renger, W., Dörnbrack, A., Leutbecher, M., Volkert, H., Tsias, A., Carslaw, K. S. and Peter, T. 1999. Model guided Lagrangian observation and simulation of mountain polar stratospheric clouds. *J. Geophys. Res*. in press.